PHYSICAL REVIEW D **80,** 014022 (2009)

QCD corrections to associated production of $t\bar{t}\gamma$ at hadron colliders

Duan Peng-Fei, Ma Wen-Gan, Zhang Ren-You, Han Liang, Guo Lei, and Wang Shao-Ming

Department of Modern Physics, University of Science and Technology of China (USTC), Hefei, Anhui 230026, China

(Received 17 May 2009; published 29 July 2009)

We report on the next-to-leading order (NLO) QCD computation of top-quark pair production in association with a photon at the Fermilab Tevatron RUN II and CERN Large Hadron Collider. We describe the impact of the complete NLO QCD radiative corrections to this process, and provide the predictions of the leading order (LO) and NLO integrated cross sections, distributions of the transverse momenta of the top quark and photon for the LHC and Tevatron, and the LO and NLO forward-backward top-quark charge asymmetries for the Tevatron. We investigate the dependence of the LO and NLO cross sections on the renormalization/factorization scale, and find the scale dependence of the LO cross section is obviously improved by the NLO QCD corrections. The K-factor of the NLO QCD correction is 0.977 (1.524) for the Tevatron (LHC).

DOI: 10.1103/PhysRevD.80.014022 PACS numbers: 14.65.Ha, 12.38.Bx, 14.70.Bh

I. INTRODUCTION

The top quark was discovered by the CDF and D0 collaborations at Fermilab Tevatron in 1995 [1,2]. It opens up a new research field of top physics, and confirms again the three-generation structure of the standard model (SM) [3,4]. Among all the elementary particles discovered up to now [5,6], the top-quark mass term breaks the electroweak (EW) gauge symmetry maximally due to its huge mass, and the detailed physics of the top quark may be significantly different from the predictions provided by the SM. But until now our knowledge about the top quark's properties has been still limited [7]. For example, the couplings of the top quark to a photon and a Z^0 boson have not yet been directly measured [8,9], while the precise measurement of the production and decay of the top quark may be significant in searching for new physics beyond the SM.

In recent years there have been many works devoted to the study of the top-quark couplings. The studies for probing the top-quark couplings $t\bar{t}\gamma$ and $t\bar{t}Z^0$ at hadron colliders at LO were carried out in Ref. [10], the calculations for the process $e^+e^- \to t\bar{t}Z^0$ at LO, QCD, and EW NLO are provided in Refs. [11], and the one-loop SM QCD and the supersymmetric QCD effects in the process of $\gamma\gamma \to t\bar{t}Z^0$ at the ILC was investigated in Ref. [12]. The SM couplings of $t\bar{t}V$ ($V = \gamma$, Z^0) may be modified by the new interactions and that would lead to abundant phenomena of new physics. For example, if the top quark was a composite object, there would be an anomalously large $t\bar{t}\gamma$ event rate at colliders, due to deexcitation of high-energetic top state [13]. And if there exists nonstandard CP violation, in particular, Higgs sector CP violation, a sizable top-quark (weak) electric dipole moment could be induced [14]. Other relevant references [9,15–17] indicate that the vector and axial form factors in the coupling of the top quark and neutral gauge boson V ($= \gamma$, Z^0) should be probed precisely in order to find the signatures of a certain model of dynamical EW breaking.

At a linear collider, it is not easy to obtain the information about the individual EW neutral coupling $t\bar{t}V$ ($V = Z^0$, γ) from the precise measurement of the top-pair production at a linear collider because of the hardness in distinguishing the contributions from the $t\bar{t}Z^0$ and $t\bar{t}\gamma$ couplings. At a hadron collider, it is impossible to measure the EW neutral couplings via $q\bar{q} \to \gamma^*/Z^* \to t\bar{t}$ due to the strong interaction process $q\bar{q}(gg) \to g^* \to t\bar{t}$. Instead, they can be measured in QCD $t\bar{t}Z^0/\gamma$ production and radiative top-quark decays in $t\bar{t}$ events ($t\bar{t} \to \gamma W^+W^- b\bar{b}$). Each of the processes is sensitive to the EW coupling between the top quark and the emitted Z^0-boson (or photon). In the work of [18] it is concluded that it will be possible to probe the $t\bar{t}\gamma$ coupling at a few percent level at the LHC. Since the LO predictions in the QCD expansion for the channels $pp(p\bar{p}) \to t\bar{t}Z^0(\gamma) + X$ at hadron colliders contain significant theoretical uncertainty, it is important to improve the theoretical prediction in order to accommodate the experimental measurement of the top-quark couplings. Recently, the NLO QCD correction to $t\bar{t}Z^0$ production at the LHC has been calculated in Ref. [19].

Our study in this work corresponds to the investigation on the production of the top-quark pair associated with a photon at the Fermilab Tevatron Run II and the CERN LHC in both LO and NLO QCD approximations. It is arranged as follows: In Sec. II we provide descriptions of the analytical calculations. In Sec. III we present some numerical results and discussions, and finally a short summary is given.

II. DESCRIPTION OF THE CALCULATION

In the calculations at the LO and NLO of the α_s expansion, we use the 't Hooft-Feynman gauge, employ the

FEYNARTS3.4 package [20] to generate Feynman diagrams and their corresponding amplitudes. The LO amplitudes are precessed by adopting FORMCALC5.4 programs [21]. In the calculation for virtual corrections, the one-loop amplitudes involving UV and IR singularities are handled analytically by using our modified FORMCALC programs, and are output in FORTRAN code with the UV and IR "$\epsilon \times N$-point integrals" terms remained unprocessed. The output is further processed numerically by using our developed FORTRAN subroutines for calculating N-point integrals to extract the remaining finite $\epsilon\frac{1}{\epsilon}$ terms. In these FORTRAN codes the IR singularities are separated from the IR-finite remainder by adopting the expressions for the IR singularity in N-point integrals ($N \geq 3$) in terms of 3-point integrals [22].

A. Born approximation

We consider five partonic processes, which contribute to the process of top-pair production associated with a photon at LO for hadron colliders. They are $gg \to t\bar{t}\gamma$ and $q\bar{q} \to t\bar{t}\gamma$ ($q = u, d, c, s$) production channels. We take the constraint for the transverse momentum for radiated photon as $p_T^{(\gamma)} > p_{T,\mathrm{cut}}^{(\gamma)}$, e.g., $p_{T,\mathrm{cut}}^{(\gamma)} = 20$ GeV. We express these partonic reactions as

$$q(p_1) + \bar{q}(p_2) \to t(p_3) + \bar{t}(p_4) + \gamma(p_5), \quad (q = u, d, s, c), \tag{2.1}$$

and

$$g(p_1) + g(p_2) \to t(p_3) + \bar{t}(p_4) + \gamma(p_5), \tag{2.2}$$

where we denote the external four momenta by p_i ($i = 1, \ldots, 5$) for the partonic processes $q\bar{q} \to t\bar{t}\gamma$ and $gg \to t\bar{t}\gamma$, separately. There are 4 LO Feynman diagrams for partonic process $q\bar{q} \to t\bar{t}\gamma$ (shown in Fig. 1), and 8 tree-level diagrams for the $gg \to t\bar{t}\gamma$ partonic process (shown in Fig. 2). Despite being massless for photon and light quarks ($q = u, d, s$), the cross sections for the above partonic processes are still "infrared safe" due to our constraint for the photon transverse momentum.

The expression of LO cross section for the partonic processes $q\bar{q} \to t\bar{t}\gamma$ and $gg \to t\bar{t}\gamma$ have the forms, respectively, as

$$\begin{aligned} d\hat{\sigma}^0_{q\bar{q}} &= \frac{1}{4}\frac{1}{9}\frac{(2\pi)^4}{2\hat{s}} \sum_{\mathrm{spin}}^{\mathrm{color}} |\mathcal{M}^{q\bar{q}}_{\mathrm{LO}}|^2 d\Omega_3^{q\bar{q}}, \\ d\hat{\sigma}^0_{gg} &= \frac{1}{4}\frac{1}{64}\frac{(2\pi)^4}{2\hat{s}} \sum_{\mathrm{spin}}^{\mathrm{color}} |\mathcal{M}^{gg}_{\mathrm{LO}}|^2 d\Omega_3^{gg}, \end{aligned} \tag{2.3}$$

where the factors $\frac{1}{4}$, $\frac{1}{9}$ and factors $\frac{1}{4}$, $\frac{1}{64}$ in Eqs. (2.3) come from the averaging over the spins and colors of the initial partons, respectively, $\hat{s}$ is the partonic center-of-mass energy squared, $\mathcal{M}^{q\bar{q}}_{\mathrm{LO}}$ and $\mathcal{M}^{gg}_{\mathrm{LO}}$ are the amplitudes of all the tree-level diagrams for the partonic processes $q\bar{q} \to t\bar{t}\gamma$ and $gg \to t\bar{t}\gamma$, respectively. In the above two equations the

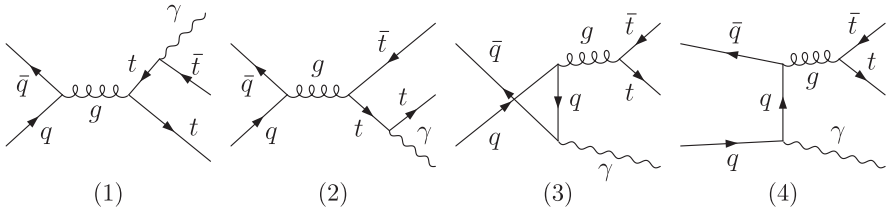

FIG. 1. The LO Feynman diagrams for the $q\bar{q} \to t\bar{t}\gamma$ ($q = u, d, s, c$) partonic process.

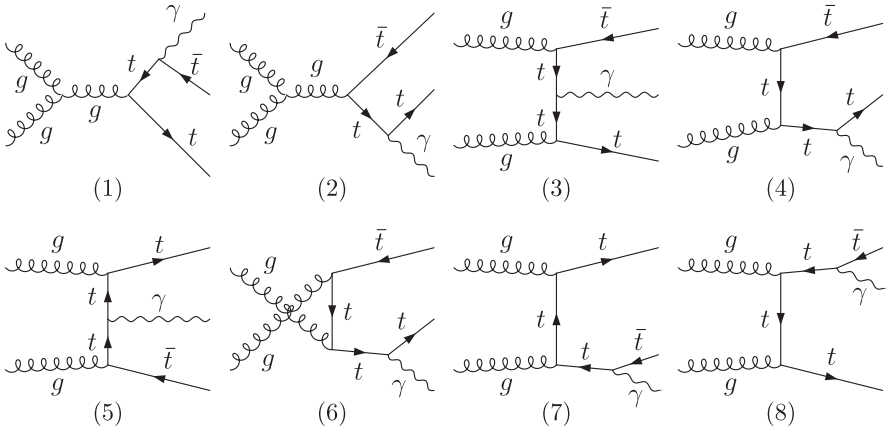

FIG. 2. The LO Feynman diagrams for the $gg \to t\bar{t}\gamma$ partonic process.

summations are taken over the spins and colors of all the relevant particles in the $q\bar{q} \to t\bar{t}\gamma$ and $gg \to t\bar{t}\gamma$ partonic processes. The phase-space elements $d\Omega_3^{q\bar{q}}$ and $d\Omega_3^{gg}$ in Eqs. (2.3) is expressed as

$$d\Omega_3^{q\bar{q},gg} = \delta^{(4)}\Big(p_1 + p_2 - \sum_{i=3}^{5} p_i\Big)\prod_{j=3}^{5}\frac{d^3\mathbf{p}_j}{(2\pi)^3 2E_j}. \quad (2.4)$$

According to the factorization theorem for hard scattering processes in QCD, the LO differential cross section for the process $p\bar{p}(pp) \to t\bar{t}\gamma + X$ at the Tevatron (LHC) can be obtained by performing the following integration of the differential cross section for the partonic processes $q\bar{q} \to t\bar{t}\gamma$ and $gg \to t\bar{t}\gamma$ over the initial partonic luminosities [see Eq. (2.5)].

$$\begin{aligned} d\sigma_{\rm LO} = & \sum_{ij=u\bar{u},d\bar{d}}^{s\bar{s},c\bar{c},gg}\int_0^1 dx_1\int_0^1 dx_2\,\frac{1}{1+\delta_{ij}} \\ & \times\Big[G_{i/P_1}(x_1,\mu_f)G_{j/P_2}(x_2,\mu_f)\frac{d\hat{\sigma}_{ij}^0}{d\hat{y}_t} \\ & + G_{j/P_1}(x_1,\mu_f)G_{i/P_2}(x_2,\mu_f)\frac{d\hat{\sigma}_{ji}^0}{d\hat{y}_t}\Big]dy_t, \quad (2.5) \end{aligned}$$

where y_t and $\hat{y}_t$ are the rapidities of the top quark in the proton-(anti)proton and partonic center-of-mass systems, respectively, ($y_t = \frac{1}{2}\ln(\frac{E^t + p_z^t}{E^t - p_z^t})$, $\hat{y}_t = \frac{1}{2}\ln(\frac{\hat{E}^t + \hat{p}_z^t}{\hat{E}^t - \hat{p}_z^t})$). The direction of the z-axis of the hadronic center-of-mass system is defined as the orientation of incoming hardron P_1 (for the parent process $P_1P_2 \to t\bar{t}\gamma + X$), while the z-axis of the partonic center-of-mass system is set as the orientation of radiated parton i (or j) from P_1 [for the partonic process ij(or ji) $\to t\bar{t}\gamma$]. The differential cross sections $\frac{d\hat{\sigma}_{ij}^0}{d\hat{y}_t}$ and $\frac{d\hat{\sigma}_{ji}^0}{d\hat{y}_t}$ are expressed in their own partonic center-of-mass frames, respectively. Under a boost in the z-direction to a frame with velocity β, we have $y_t = \hat{y}_t - \tanh^{-1}\beta$ and $dy_t = d\hat{y}_t$. $G_{i(j)/A}(x,\mu_f)$ ($i = u, d, s, c, g$, $j = \bar{u}, \bar{d}, \bar{s}, \bar{c}, g$) are the parton distribution functions (PDFs) of (anti)proton A ($= P_1, P_2$) which describe the probability to find a parton $i(j)$ with four-momentum xp_A in (anti)proton A. The partonic colliding energy squared $\hat{s} = x_1x_2s$, where s is defined as the center-of-mass energy squared of the proton-(anti)proton collision. μ_f is the factorization energy scale. In our LO calculations, we adopt the CTEQ6L1 PDFs [23].

Our LO calculation shows when we take $p_{T,\rm cut}^{(\gamma)} = 20$ GeV, the LO integrated cross section for the $t\bar{t}\gamma$ production is dominated by the gluon-gluon fusion partonic channel with about 66.3% at the LHC, while about 99.3% is contributed by the $q - \bar{q}$ ($q = u, d$) annihilation partonic channels at the Tevatron RUN II.

B. NLO QCD corrections

The NLO QCD corrections to the $pp(p\bar{p}) \to t\bar{t}\gamma + X$ process are contributed distinctly by the following four parts:

(1) the real gluon emission partonic processes $q\bar{q}, gg \to t\bar{t}\gamma g$, ($q = u, d, s, c$).
(2) the real light-(anti)quark emission partonic processes $q(\bar{q})g \to t\bar{t}\gamma q(\bar{q})$, ($q = u, d, s$).
(3) the virtual corrections at the NLO to the partonic processes $q\bar{q}, gg \to t\bar{t}\gamma$, ($q = u, d, s, c$).
(4) the collinear counterterms of the PDF.

In all the NLO calculations we use the dimensional regularization (DR) method in $D = 4 - 2\epsilon$ dimensions to isolate the UV and IR singularities. To describe the cancellations of the IR singularities in our calculations more clearly, we decompose the collinear counterterms of the PDF, $\delta G_{i/P}(x,\mu_f)$ ($P = p, \bar{p}$; $i = g, u, \bar{u}, d, \bar{d}, s, \bar{s}$), into two parts: the collinear gluon emission part $\delta G_{i/P}^{(\rm gluon)}(x,\mu_f)$ and the collinear light-quark emission part $\delta G_{i/P}^{(\rm quark)}(x,\mu_f)$. Their analytical expressions are presented as follows.

$$\begin{aligned} \delta G_{q(g)/P}(x,\mu_f) = & \delta G_{q(g)/P}^{(\rm gluon)}(x,\mu_f) + \delta G_{q(g)/P}^{(\rm quark)}(x,\mu_f), \\ & (q = u, \bar{u}, d, \bar{d}, s, \bar{s}), \end{aligned} \quad (2.6)$$

where

$$\begin{aligned} \delta G_{q(g)/P}^{(\rm gluon)}(x,\mu_f) = & \frac{1}{\epsilon}\Big[\frac{\alpha_s}{2\pi}\frac{\Gamma(1-\epsilon)}{\Gamma(1-2\epsilon)}\Big(\frac{4\pi\mu_r^2}{\mu_f^2}\Big)^{\epsilon}\Big] \\ & \times\int_z^1\frac{dz}{z}P_{qq(gg)}(z)G_{q(g)/P}(x/z,\mu_f), \\ \delta G_{q/P}^{(\rm quark)}(x,\mu_f) = & \frac{1}{\epsilon}\Big[\frac{\alpha_s}{2\pi}\frac{\Gamma(1-\epsilon)}{\Gamma(1-2\epsilon)}\Big(\frac{4\pi\mu_r^2}{\mu_f^2}\Big)^{\epsilon}\Big] \\ & \times\int_z^1\frac{dz}{z}P_{qg}(z)G_{g/P}(x/z,\mu_f), \\ \delta G_{g/P}^{(\rm quark)}(x,\mu_f) = & \frac{1}{\epsilon}\Big[\frac{\alpha_s}{2\pi}\frac{\Gamma(1-\epsilon)}{\Gamma(1-2\epsilon)}\Big(\frac{4\pi\mu_r^2}{\mu_f^2}\Big)^{\epsilon}\Big] \\ & \times\sum_{q=u,\bar{u}}^{d,\bar{d},s,\bar{s}}\int_z^1\frac{dz}{z}P_{gq}(z)G_{q/P}(x/z,\mu_f). \end{aligned} \quad (2.7)$$

The virtual corrections to the processes $pp(p\bar{p}) \to q\bar{q}$, $gg \to t\bar{t}\gamma + X$ contain both soft and collinear IR singularities. These singularities can be canceled exactly by adding the contributions of the real gluon emission processes $q\bar{q}$, $gg \to t\bar{t}\gamma g$ and the collinear gluon emission part of the PDF counterterms $\delta G_{q(g)/P}^{(\rm gluon)}$. The real light-quark emission processes $q(\bar{q})g \to t\bar{t}\gamma q(\bar{q})$ contain only the collinear IR singularities. It can be canceled by the contributions of the

collinear light-quark emission part of the PDF counterterms $\delta G^{(\mathrm{quark})}_{q(g)/P}$ exactly. All of these cancellations are verified numerically in our numerical calculations. The explicit expressions for the splitting functions $P_{ij}(z)$, $(ij = qq, qg, gq, gg)$ can be found in Ref. [24].

1. Real gluon emission corrections

We denote the partonic processes with real gluon emissions as

$$\begin{aligned} &q(p_1) + \bar{q}(p_2) \to t(p_3) + \bar{t}(p_4) + \gamma(p_5) + g(p_6), \\ &g(p_1) + g(p_2) \to t(p_3) + \bar{t}(p_4) + \gamma(p_5) + g(p_6). \end{aligned} \tag{2.8}$$

The real gluon emission partonic process $q\bar{q} \to t\bar{t}\gamma g$ includes 24 LO graphs shown in Fig. 3, and the $gg \to t\bar{t}\gamma g$ subprocess involves 50 LO graphs (shown in Fig. 4). The figures (1)–(10) in Fig. 4 are s-channel diagrams, the Figs. 4 (11)–(30) are t-channel diagrams. The u-channel diagrams for the $gg \to t\bar{t}\gamma g$ subprocess are not drawn in Fig. 4, but can be obtained by exchanging incoming gluons in each t-channel diagram in Fig. 4. The process $c\bar{c} \to t\bar{t}\gamma g$ contains only the soft IR singularity, while $q\bar{q} \to t\bar{t}\gamma g$, $(q = u, d, s)$ and $gg \to t\bar{t}\gamma g$ contain both soft and IR singularities. The soft IR singularities can be extracted by adopting the two cutoff phase-space slicing (TCPSS) methods [24], respectively. The soft IR singularities in the partonic processes $q\bar{q} \to t\bar{t}\gamma g$, $(q = u, d, s, c)$, and $gg \to t\bar{t}\gamma g$ at the LO cancel the corresponding soft IR singularities arising from the one-loop virtual corrections to $q\bar{q} \to t\bar{t}\gamma$, $(q = u, d, s, c)$ and $gg \to t\bar{t}\gamma$ processes, respectively.

We split the phase-space of the $gg(q\bar{q}) \to t\bar{t}\gamma g$, $(q = u, d, s, c)$ partonic process into two regions, $E_6 \le \delta_s\sqrt{\hat{s}}/2$ (soft gluon region) and $E_6 > \delta_s\sqrt{\hat{s}}/2$ (hard gluon region). Except for the $c\bar{c} \to t\bar{t}\gamma g$ process, the hard gluon region is divided into hard collinear region (HC) ($-\hat{t}_{16}$ or $-\hat{t}_{26} < \delta_c\hat{s}$) and hard noncollinear ($\overline{\mathrm{HC}}$) region ($-\hat{t}_{16}$ or $-\hat{t}_{26} \ge \delta_c\hat{s}$), where $\hat{t}_{ij} = (p_i - p_j)^2$ and $(p_i - p_j)^2$ for the $q\bar{q} \to t\bar{t}\gamma g$ and $gg \to t\bar{t}\gamma g$, respectively. Then the cross sections for the real gluon emission partonic processes can be expressed as

$$\begin{aligned} \hat{\sigma}^R_{g,ij}(ij \to t\bar{t}\gamma g) &= \hat{\sigma}^S_{g,ij} + \hat{\sigma}^H_{g,ij}, \\ &(ij = u\bar{u}, d\bar{d}, s\bar{s}, c\bar{c}, gg) \\ \hat{\sigma}^H_{g,ij}(ij \to t\bar{t}\gamma g) &= \hat{\sigma}^{\mathrm{HC}}_{g,ij} + \hat{\sigma}^{\overline{\mathrm{HC}}}_{g,ij}, \\ &(ij = u\bar{u}, d\bar{d}, s\bar{s}, gg) \end{aligned} \tag{2.9}$$

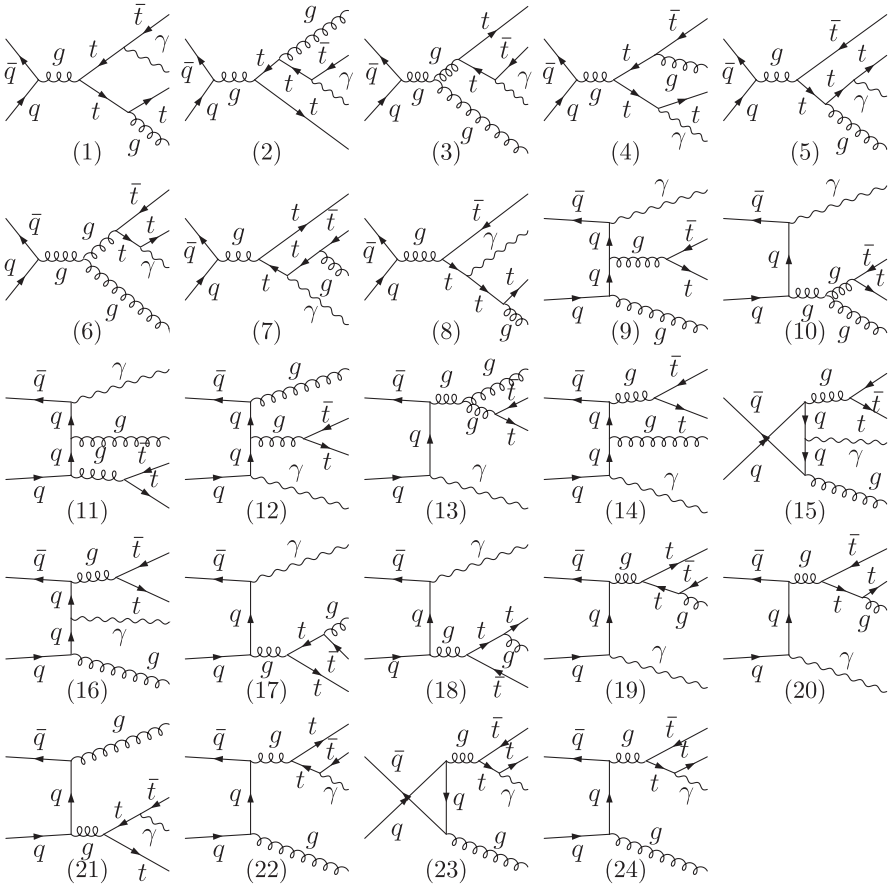

FIG. 3. The LO Feynman diagrams for the real gluon emission partonic process $q\bar{q} \to t\bar{t}\gamma g$ $(q = u, d, s, c)$.

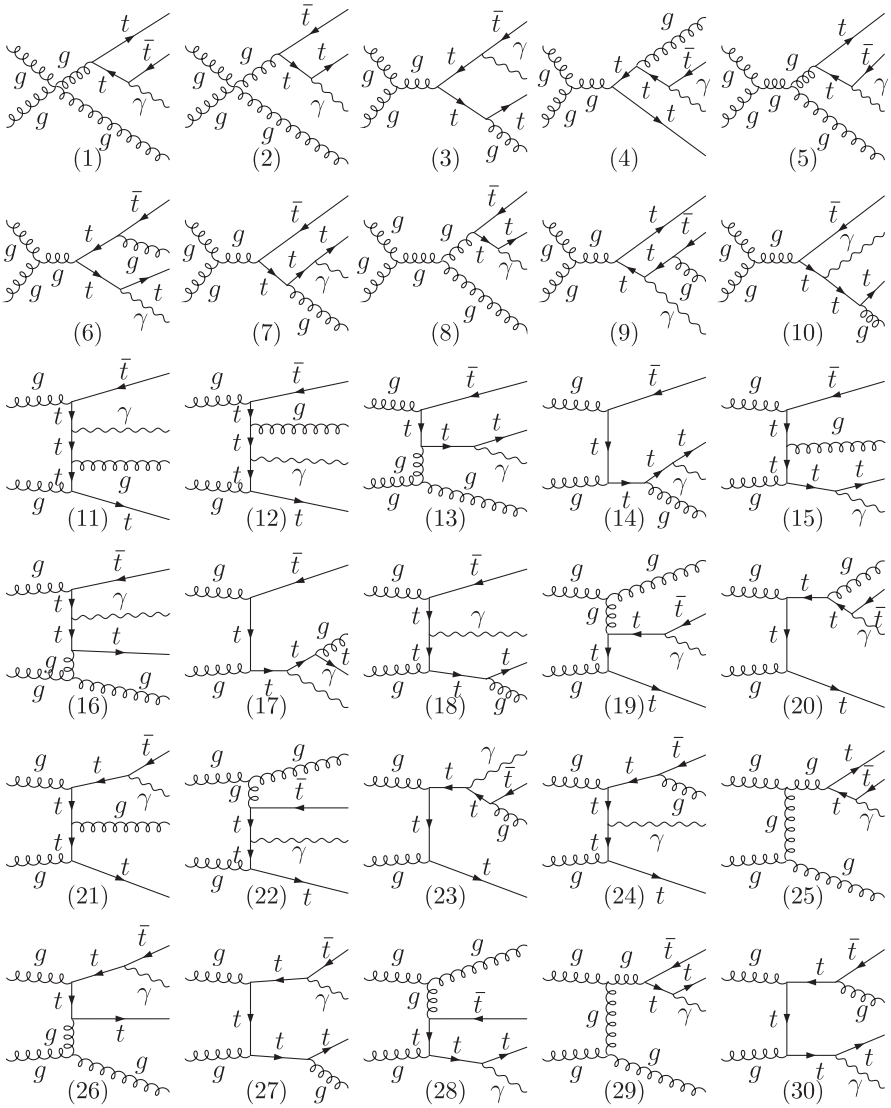

FIG. 4. The LO Feynman diagrams for the real gluon emission partonic process $gg \to t\bar{t}\gamma g$. The diagrams obtained by exchanging two initial gluon lines in (11)–(30) are not drawn.

The differential cross section for the partonic processes $q\bar{q} \to t\bar{t}\gamma g$ in the soft region is given as

$$
\begin{aligned}
d\hat{\sigma}^S_{g,q\bar{q}} &= -\frac{\alpha_s}{2\pi}\Big[\frac{1}{6}(g_{12}+g_{34}) - \frac{7}{6}(g_{13}+g_{24}) \\
&\quad - \frac{1}{3}(g_{14}+g_{23})\Big] d\hat{\sigma}^0_{q\bar{q}} \\
&= \Big[\frac{\alpha_s}{2\pi}\frac{\Gamma(1-\epsilon)}{\Gamma(1-2\epsilon)}\Big(\frac{4\pi\mu_r}{\hat{s}}\Big)^{\epsilon}\Big] \\
&\quad \times \Big(\frac{A^S_{2,q\bar{q}}}{\epsilon^2} + \frac{A^S_{1,q\bar{q}}}{\epsilon} + A^S_{0,q\bar{q}}\Big) d\hat{\sigma}^0_{q\bar{q}},
\end{aligned}
\tag{2.10}
$$

where $d\hat{\sigma}^0_{ij}$ are the LO differential cross sections for the partonic processes $ij \to t\bar{t}\gamma$, $(ij = u\bar{u}, d\bar{d}, s\bar{s}, c\bar{c})$. The soft integrals g_{ij} $(i = 1, 2, 3,\ j = 2, 3, 4)$ are defined as

$$
\begin{aligned}
g_{ij}(p_i, p_j) &= \frac{(2\pi\mu_r)^{2\epsilon}}{2\pi}\int_{E_6 \le \delta_s\sqrt{\hat{s}}/2} \frac{d^{D-1}\mathbf{p_6}}{E_6} \\
&\quad \times \Big[\frac{2(p_i\cdot p_j)}{(p_i\cdot p_6)(p_j\cdot p_6)} - \frac{p_i^2}{(p_i\cdot p_j)^2} \\
&\quad - \frac{p_j^2}{(p_j\cdot p_6)^2}\Big].
\end{aligned}
\tag{2.11}
$$

The explicit expressions for the soft integrals $g_{ij}(p_i, p_j)$ relevant to our calculations for the $q\bar{q}$, $gg \to t\bar{t}\gamma g$ partonic processes, can be found in Ref. [25]. By using Eqs. (2.10) and (2.11) and the related soft integral expressions, we can express the coefficients $A^S_{2,q\bar{q}}$ and $A^S_{1,q\bar{q}}$ in Eq. (2.10) for the massless $q\bar{q}$-fusion processes $q\bar{q} \to t\bar{t}\gamma g$ $(q = u, d, s)$ in the forms as

$$A^S_{2,q\bar{q}} = \frac{8}{3},$$
$$A^S_{1,q\bar{q}} = \frac{8}{3} - \frac{16}{3}\delta_s - \frac{1}{3}\frac{p_3\cdot p_4}{\lambda^{1/2}(s_{34}, m_t^2, m_t^2)}\log(\sigma_{34}\sigma_{43}) - \frac{7}{3}\left(\log\frac{p_1\cdot p_3}{p_1^0 m_t} + \log\frac{p_2\cdot p_4}{p_2^0 m_t}\right) - \frac{2}{3}\left(\log\frac{p_2\cdot p_3}{p_2^0 m_t} + \log\frac{p_1\cdot p_4}{p_1^0 m_t}\right). \tag{2.12}$$

And for the massive $c\bar{c}$-fusion partonic process $c\bar{c} \to t\bar{t}\gamma g$, we get

$$A^S_{2,q\bar{q}} = 0,$$
$$A^S_{1,q\bar{q}} = \frac{16}{3} - \frac{1}{3}\left(\frac{p_1\cdot p_2}{\lambda^{1/2}(s_{12}, m_c^2, m_c^2)}\log(\sigma_{12}\sigma_{21}) + \frac{p_3\cdot p_4}{\lambda^{1/2}(s_{34}, m_t^2, m_t^2)}\log(\sigma_{34}\sigma_{43})\right) + \frac{7}{3}\left(\frac{p_1\cdot p_3}{\lambda^{1/2}(s_{13}, m_c^2, m_t^2)}\log(\sigma_{13}\sigma_{31}) + \frac{p_2\cdot p_4}{\lambda^{1/2}(s_{24}, m_c^2, m_t^2)}\log(\sigma_{24}\sigma_{42})\right) + \frac{2}{3}\left(\frac{p_1\cdot p_4}{\lambda^{1/2}(s_{14}, m_c^2, m_t^2)}\log(\sigma_{14}\sigma_{41}) + \frac{p_2\cdot p_3}{\lambda^{1/2}(s_{23}, m_c^2, m_t^2)}\log(\sigma_{23}\sigma_{32})\right). \tag{2.13}$$

with $\sigma_{ij} = \frac{1-\rho_{ij}}{1+\rho_{ij}}$, $\rho_{ij} = \frac{\lambda^{1/2}(s_{ij}, m_i^2, m_j^2)}{s_{ij}+m_i^2-m_j^2}$ and $\lambda^{1/2}(s_{ij}, m_i^2, m_j^2) = \sqrt{(s_{ij}+m_i^2-m_j^2)^2 - 4s_{ij}m_i^2}$.

For the $gg \to t\bar{t}\gamma g$ partonic process in the soft region, we have

$$d\hat{\sigma}^S_{g,gg} = \frac{\alpha_s}{12\pi}\bar{\sum}\Big[\left(\frac{256}{3}D_1 + 16D_3\right)|\mathcal{M}_1^{gg}|^2 + \left(\frac{256}{3}D_2 + 16D_4\right)|\mathcal{M}_2^{gg}|^2 + \left(-\frac{32}{3}D_1 + 16D_3\right)2\,\mathbf{Re}(\mathcal{M}_1^{gg\dagger}\cdot\mathcal{M}_2^{gg})\Big]d\Omega_3^{gg}, \tag{2.14}$$

where the summation is taken over the spins and colors of initial and final states, and the bar over the summation represents taking the average over the spins and colors of initial partons, and

$$\mathcal{M}_1^{gg} = \mathcal{M}_t^{gg} + \tfrac{1}{2}\mathcal{M}_s^{gg}, \qquad \mathcal{M}_2^{gg} = \mathcal{M}_u^{gg} - \tfrac{1}{2}\mathcal{M}_s^{gg}, \tag{2.15}$$

$\mathcal{M}_s^{gg}$, $\mathcal{M}_t^{gg}$, and $\mathcal{M}_u^{gg}$ are the amplitudes for s-, t-, and u-channel diagrams of partonic process $gg \to t\bar{t}\gamma$ separately, and

$$\mathcal{M}^{gg}_{\mathrm{LO}} = (\tfrac{2}{3}C_1^{gg} + C_2^{gg} + C_3^{gg})\mathcal{M}_1^{gg} + (\tfrac{2}{3}C_1^{gg} - C_2^{gg} + C_3^{gg})\mathcal{M}_2^{gg}. \tag{2.16}$$

The color factors are expressed as

$$C_1^{gg} = \delta^{c_1c_2}\mathbf{1}, \qquad C_2^{gg} = if^{c_1c_2c}\lambda^c, \qquad C_3 = d^{c_1c_2c}\lambda^c, \tag{2.17}$$

where f^{abc} and d^{abc} are antisymmetric and symmetric $SU(3)$ structure constants, respectively, $\mathbf{1}$ and λ^c are identity and Gell-Mann matrices. c_1, c_2 are the color indices of initial gluons, c is the color index of propagator gluon and

$$D_1 = 9g_{12} + 9g_{13} + 9g_{24} - g_{34},$$
$$D_2 = 9g_{12} + 9g_{23} + 9g_{14} - g_{34},$$
$$D_3 = 6(g_{12} - g_{14} - g_{23} + g_{34}),$$
$$D_4 = 6(g_{12} - g_{13} - g_{24} + g_{34}). \tag{2.18}$$

The cross sections for the processes $pp(p\bar{p}) \to ij \to t\bar{t}\gamma g + X$, $(ij = u\bar{u}, d\bar{d}, s\bar{s}, gg)$ in the hard noncollinear region, $\hat{\sigma}^{\overline{\mathrm{HC}}}_{g,ij}$, and $pp(p\bar{p}) \to c\bar{c} \to t\bar{t}\gamma g + X$ in the hard region, $\hat{\sigma}^{H}_{g,c\bar{c}}$, are finite and can be calculated by using Monte Carlo method. The differential cross section in the hard collinear region, $d\sigma^{\mathrm{HC}}_{g,ij}$, can be obtained by using

$$d\sigma^{\mathrm{HC}}_{g,ij} = \frac{1}{1+\delta_{ij}}\left[\frac{\alpha_s}{2\pi}\frac{\Gamma(1-\epsilon)}{\Gamma(1-2\epsilon)}\left(\frac{4\pi\mu_r^2}{\hat{s}}\right)^{\epsilon}\right]\left(-\frac{1}{\epsilon}\right)\delta_c^{-\epsilon}\int_0^1 dx_1\int_0^1 dx_2 \times\Big\{\Big[\int_{x_1}^{1-\delta_s}\frac{dz}{z}\left(\frac{1-z}{z}\right)^{-\epsilon}P_{ii}(z,\epsilon)G_{i/P_1}(x_1/z,\mu_f)G_{j/P_2}(x_2,\mu_f) + \int_{x_2}^{1-\delta_s}\frac{dz}{z}\left(\frac{1-z}{z}\right)^{-\epsilon}P_{jj}(z,\epsilon)G_{i/P_1}(x_1,\mu_f)G_{j/P_2}(x_2/z,\mu_f)\Big]d\hat{\sigma}^0_{ij} + (i\leftrightarrow j)\Big\}, \tag{2.19}$$

where $G_{i(j)/P}(x, \mu_f)$ is the PDF of parton $i(j)$, and P refers to (anti)proton. $P_{ii}(z, \epsilon)$ ($i = q$ for $q - \bar{q}$ annihilation subprocess and $i = g$ for $g - g$ fusion subprocess) are the D-dimensional unregulated ($z < 1$) splitting functions related to the usual Altarelli-Parisi splitting kernel [26]. They can be written explicitly as

$$P_{ii}(z, \epsilon) = P_{ii}(z) + \epsilon P'_{ii}(z), \qquad (i = q, g),$$

$$\begin{aligned} P_{qq}(z) &= C_F \frac{1+z^2}{1-z}, \\ P'_{qq}(z) &= -C_F(1-z), \\ P_{gg}(z) &= 2N\left[\frac{z}{1-z} + \frac{1-z}{z} + z(1-z)\right], \\ P'_{gg}(z) &= 0, \end{aligned} \tag{2.20}$$

where $N = 3$ is the color number, $C_F = 4/3$.

2. Real light-(anti)quark emission corrections

Since the LO contributions from the real light-(anti) quark emission partonic processes $q(\bar{q})g \to t\bar{t}\gamma q(\bar{q})$ are at the same α_s order as previous real gluon emission partonic processes $q\bar{q} \to t\bar{t}\gamma g$ and $gg \to t\bar{t}\gamma g$ in perturbation theory, according to the Kinoshita-Lee-Nauenberg (KLN) theorem [27], we should consider these subprocesses too. The LO Feynman diagrams for the partonic processes $q(\bar{q})g \to t\bar{t}\gamma q(\bar{q})$ ($q = u, d, s$) can be obtained by exchanging initial (anti)quark and final gluon in corresponding diagrams in Fig. 3.

In order to avoid the additional IR singularity at the LO for the partonic processes $q(\bar{q})g \to t\bar{t}\gamma q(\bar{q})$ ($q = u, d, s$) due to the radiated photon from a massless light-(anti) quark, we take a photon transverse momentum cut and an angle cut between the jet and photon, e.g. $p_T^{(\gamma)} > 20$ GeV and $\theta_{\gamma,\text{jet}} > \theta_{\gamma,\text{jet}}^{\text{cut}} = 3°$ [in the proton-(anti)proton center-of-mass system].[1] Then these partonic processes contain only the initial state collinear singularities induced by strong interaction. Splitting the phase-space into collinear and noncollinear regions by introducing a cutoff δ_c, we can express the cross sections for the partonic processes $qg \to t\bar{t}\gamma q$ and $\bar{q}g \to t\bar{t}\gamma\bar{q}$ as

$$\hat{\sigma}^R(q(\bar{q})g \to t\bar{t}\gamma q(\bar{q})) = \hat{\sigma}^R_{q(\bar{q})g} = \hat{\sigma}^C_{q(\bar{q})g} + \hat{\sigma}^{\bar{C}}_{q(\bar{q})g} \tag{2.21}$$

The cross sections in the noncollinear region, $\hat{\sigma}^{\bar{C}}_{q(\bar{q})g}$, are finite and can be evaluated in four dimensions by using Monte Carlo method. The differential cross sections in the collinear region for the $pp \to q(\bar{q})g \to t\bar{t}\gamma q(\bar{q}) + X$, ($q = u, d, s$) processes, $d\sigma^C_{q(\bar{q})}$, can be written as

$$\begin{aligned} d\sigma^C_q = &\left[\frac{\alpha_s}{2\pi}\frac{\Gamma(1-\epsilon)}{\Gamma(1-2\epsilon)}\left(\frac{4\pi\mu_r^2}{\hat{s}}\right)^{\epsilon}\right]\left(-\frac{1}{\epsilon}\right)\delta_c^{-\epsilon}\int_0^1 dx_1\int_0^1 dx_2 \\ &\times\left\{\left[\int_{x_1}^1 \frac{dz}{z}\left(\frac{1-z}{z}\right)^{-\epsilon} P_{qg}(z,\epsilon) G_{g/P_1}(x_1/z, \mu_f) G_{q/P_2}(x_2, \mu_f) d\hat{\sigma}^0_{\bar{q}q}\right.\right. \\ &\left.+ \int_{x_2}^1 \frac{dz}{z}\left(\frac{1-z}{z}\right)^{-\epsilon} P_{qg}(z,\epsilon) G_{q/P_1}(x_1, \mu_f) G_{g/P_2}(x_2/z, \mu_f) d\hat{\sigma}^0_{q\bar{q}}\right] \\ &+ \left[\int_{x_1}^1 \frac{dz}{z}\left(\frac{1-z}{z}\right)^{-\epsilon} P_{gq}(z,\epsilon) G_{q/P_1}(x_1/z, \mu_f) G_{g/P_2}(x_2, \mu_f)\right. \\ &\left.\left.+ \int_{x_2}^1 \frac{dz}{z}\left(\frac{1-z}{z}\right)^{-\epsilon} P_{gq}(z,\epsilon) G_{g/P_1}(x_1, \mu_f) G_{q/P_2}(x_2/z, \mu_f)\right] d\hat{\sigma}^0_{gg}\right\}, \end{aligned} \tag{2.22}$$

and

$$d\sigma^C_{\bar{q}} = d\sigma^C_q(q \leftrightarrow \bar{q}). \tag{2.23}$$

where the splitting functions $P_{qg(gq)}(z, \epsilon)$ can be written explicitly as [26]

$$\begin{aligned} P_{qg,gq}(z,\epsilon) &= P_{qg,gq}(z) + \epsilon P'_{qg,gq}(z), \\ P_{qg}(z) &= \frac{1}{2}[z^2 + (1-z)^2], \qquad P'_{qg}(z) = -z(1-z), \\ P_{gq}(z) &= C_F\frac{1+(1-z)^2}{z}, \qquad P'_{gq}(z) = -C_F z. \end{aligned} \tag{2.24}$$

3. Virtual corrections

There are 118 diagrams for the partonic process $q\bar{q} \to t\bar{t}\gamma$ in the SM at NLO. It involves self-energy(40), vertex (32), box(14), pentagon(4) and counterterm(28) graphs. For the partonic process $gg \to t\bar{t}\gamma$ there are 306 diagrams at NLO in the SM, including self-energy(32), vertex(156),

[1] From the experimental point of view, we should apply angle cut $\theta_{\gamma,\text{jet}}^{\text{cut}}$ not only to the $pp \to q(\bar{q})g \to t\bar{t}\gamma q(\bar{q}) + X$ processes, but also the $pp \to q\bar{q}$, $gg \to t\bar{t}\gamma g + X$ processes. The subscript "jet" in $\theta_{\gamma,\text{jet}}$ represents the light-(anti) quark jet or gluon jet for the real light-(anti) quark emission processes or the real gluon emission processes.

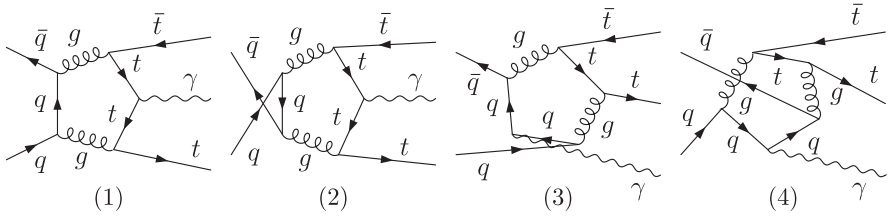

FIG. 5. The pentagon Feynman diagrams for the partonic process $q\bar{q} \to t\bar{t}\gamma$ ($q\bar{q} = u\bar{u}, d\bar{d}$).

box(66), pentagon(12) and counterterm(40) graphs. Among all these graphs the pentagon diagrams are the most complicated ones. We depict them in Fig. 5 (for partonic process $q\bar{q} \to t\bar{t}\gamma$) and Fig. 6 (for partonic process $gg \to t\bar{t}\gamma$). In the NLO calculations, we use the dimensional regularization method and adopt the modified minimal subtraction ($\overline{\text{MS}}$) scheme to renormalize the strong coupling constant and the relevant masses and fields except for the top quark and gluon, where their masses and wave functions are renormalized by applying the on-shell scheme. The total NLO QCD amplitudes of partonic processes $q\bar{q} \to t\bar{t}\gamma$ and $gg \to t\bar{t}\gamma$ are UV finite after performing the renormalization procedure. Nevertheless, they still contain soft/collinear IR singularities.

The virtual corrections to the subprocesses $q\bar{q} \to t\bar{t}\gamma$ and $gg \to t\bar{t}\gamma$ can be expressed as

$$d\hat{\sigma}^V_{q\bar{q}} = \frac{1}{4}\frac{1}{9}\frac{(2\pi)^4}{2\hat{s}} \sum_{\text{spin}}^{\text{color}} 2\,\text{Re}[\mathcal{M}^{q\bar{q}}_{\text{LO}} \mathcal{M}^{V}_{q\bar{q}}] d\Omega^{q\bar{q}}_3$$
$$d\hat{\sigma}^V_{gg} = \frac{1}{4}\frac{1}{64}\frac{(2\pi)^4}{2\hat{s}} \sum_{\text{spin}}^{\text{color}} 2\,\text{Re}[\mathcal{M}^{gg}_{\text{LO}} \mathcal{M}^{V}_{gg}] d\Omega^{gg}_3 \tag{2.25}$$

where $\mathcal{M}^{q\bar{q}}_{\text{LO}}$ and $\mathcal{M}^{gg}_{\text{LO}}$ are the LO Feynman matrices of the partonic processes $q\bar{q} \to t\bar{t}\gamma$ and $gg \to t\bar{t}\gamma$, and $\mathcal{M}^{V}_{q\bar{q}}$ and $\mathcal{M}^{V}_{gg}$ are the NLO matrices for the $q - \bar{q}$ and $g - g$ annihilation processes, separately.

The virtual correction parts of the cross sections containing soft/collinear IR singularities. As we can see later that the soft/collinear IR singularities are canceled exactly after combining the virtual corrections to the pertonic processes $pp(p\bar{p}) \to q\bar{q}(gg) \to t\bar{t}\gamma + X$ with the real gluon emission corrections and the gluon part of the PDF counterterms $\delta G^{(g)}_{q(g)/P}$ ($P = p, \bar{p}$; $q = u, \bar{u}, d, \bar{d}, s, \bar{s}$).

4. NLO QCD corrected cross section for $pp(p\bar{p}) \to t\bar{t}\gamma + X$ process

As shown in Eqs. (2.6), the PDF counterterms contain collinear IR singularities. By combining the contributions of the PDF counterterms with the hard collinear contributions of the $q\bar{q} \to t\bar{t}\gamma g$, $gg \to t\bar{t}\gamma g$, $q(\bar{q})g \to t\bar{t}\gamma q(\bar{q})$ subprocesses, we get the expression for the remaining collinear contributions to the process $pp(p\bar{p}) \to t\bar{t}\gamma + X$ in $\mathcal{O}(\alpha_s)$ order as,

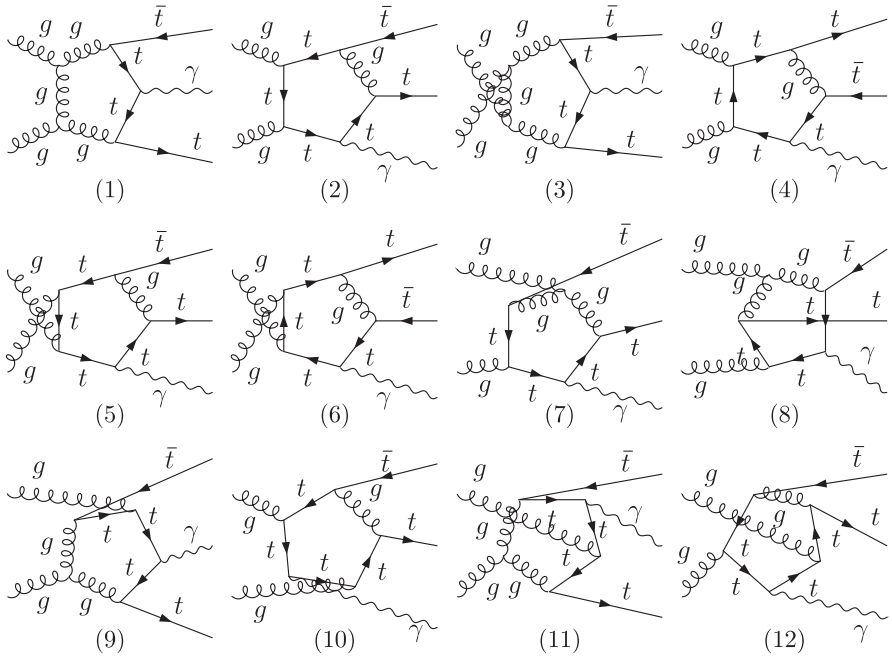

FIG. 6. The pentagon Feynman diagrams for the partonic process $gg \to t\bar{t}\gamma$.

$$d\sigma^{\rm coll} = \left[\frac{\alpha_s}{2\pi}\frac{\Gamma(1-\epsilon)}{\Gamma(1-2\epsilon)}\left(\frac{4\pi\mu_r^2}{\hat{s}}\right)^{\epsilon}\right]\sum_{ij=u\bar{u},d\bar{d}}^{s\bar{s},gg}\frac{1}{1+\delta_{ij}}\int_0^1 dx_1\int_0^1 dx_2$$
$$\times\left\{\left[\tilde{G}_{i/P_1}(x_1,\mu_f)G_{j/P_2}(x_2,\mu_f)+G_{i/P_1}(x_1,\mu_f)\tilde{G}_{j/P_2}(x_2,\mu_f)\right.\right.$$
$$\left.\left.+\sum_{\alpha=i,j}\left(\frac{A_1^{sc}(\alpha\to\alpha g)}{\epsilon}+A_0^{sc}(\alpha\to\alpha g)\right)\right]d\hat{\sigma}_{ij}^0+(i\leftrightarrow j)\right\} \quad (2.26)$$

where

$$A_1^{sc}(q\to qg)=C_F(2\ln\delta_s+3/2),\qquad A_1^{sc}(g\to gg)=2N\ln\delta_s+(11N-2n_{lf})/6, \quad (2.27)$$

$$A_0^{sc}=A_1^{sc}\ln\left(\frac{\hat{s}}{\mu_f^2}\right),\qquad \tilde{G}_{\alpha/P}(x,\mu_f)=\sum_{\alpha'}\int_x^{1-\delta_s\delta_{\alpha\alpha'}}\frac{dy}{y}G_{\alpha'/P}(x/y,\mu_f)\tilde{P}_{\alpha\alpha'}(y), \quad (2.28)$$

and

$$\tilde{P}_{\alpha\alpha'}(y)=P_{\alpha\alpha'}(y)\ln\left(\delta_c\frac{1-y}{y}\frac{\hat{s}}{\mu_f^2}\right)-P'_{\alpha\alpha'}(y), \quad (2.29)$$

where $N=3$ and $n_{lf}=5$, respectively. The explicit expressions for $P_{\alpha\alpha'}$ and $P'_{\alpha\alpha'}$ can be found in Ref. [24]. By adding the virtual correction, the soft real gluon emission corrections and the remaining collinear contributions shown in Eq. (2.26), the soft and collinear IR divergences are vanished. The final result for the total QCD correction ($\Delta\sigma^{\rm QCD}$) consists of a three-body term and a four-body term, i.e., $\Delta\sigma^{\rm QCD}=\Delta\sigma^{(3)}+\Delta\sigma^{(4)}$. The three-body term can be expressed as

$$\Delta\sigma^{(3)}=\int d\sigma^{\rm coll}+\sum_{ij=u\bar{u},d\bar{d}}^{s\bar{s},c\bar{c},gg}\frac{1}{1+\delta_{ij}}\int_0^1 dx_1\int_0^1 dx_2\int[(d\hat{\sigma}_{ij}^V+d\hat{\sigma}_{g,ij}^S)G_{i/P_1}(x_1,\mu_f)G_{j/P_2}(x_2,\mu_f)+(i\leftrightarrow j)], \quad (2.30)$$

and the four-body term has the form as

$$\Delta\sigma^{(4)}=\sum_{ij=u\bar{u},d\bar{d}}^{s\bar{s},gg}\frac{1}{1+\delta_{ij}}\int_0^1 dx_1\int_0^1 dx_2[G_{i/P_1}(x_1,\mu_f)G_{j/P_2}(x_2,\mu_f)\hat{\sigma}_{g,ij}^{\overline{\rm HC}}+(i\leftrightarrow j)]$$
$$+\int_0^1 dx_1\int_0^1 dx_2[G_{c/P_1}(x_1,\mu_f)G_{\bar{c}/P_2}(x_2,\mu_f)\hat{\sigma}_{g,c\bar{c}}^H+(c\leftrightarrow\bar{c})]$$
$$+\sum_{q=u,d,s}^{\bar{u},\bar{d},\bar{s}}\int_0^1 dx_1\int_0^1 dx_2[G_{q/P_1}(x_1,\mu_f)G_{g/P_2}(x_2,\mu_f)\hat{\sigma}_{qg}^{\bar{C}}+(q\leftrightarrow g)], \quad (2.31)$$

where $\hat{\sigma}_{g,c\bar{c}}^H$ ($\hat{s}=x_1x_2s$) and $\hat{\sigma}_{g,ij}^{\overline{\rm HC}}$ ($\hat{s}=x_1x_2s$) are the cross sections for the partonic processes $c\bar{c}\to t\bar{t}\gamma g$ and $ij\to t\bar{t}\gamma g$ ($ij=u\bar{u}$, $d\bar{d}$, $s\bar{s}$, gg) in the hard and hard noncollinear phase-space regions at the colliding energy $\hat{s}=x_1x_2s$, respectively, and $\hat{\sigma}_{qg}^{\bar{C}}(\hat{s})$ ($q=u$, $\bar{u}$, d, $\bar{d}$, s, $\bar{s}$) represent the cross sections in the noncollinear phase-space region for the partonic processes $ug\to t\bar{t}\gamma u$, $dg\to t\bar{t}\gamma d$, $\bar{u}g\to t\bar{t}\gamma\bar{u}$, $\bar{d}g\to t\bar{t}\gamma\bar{d}$, $sg\to t\bar{t}\gamma s$, and $\bar{s}g\to t\bar{t}\gamma\bar{s}$, respectively.

Finally, the QCD corrected total cross section for the $pp(p\bar{p})\to t\bar{t}\gamma+X$ process is

$$\sigma^{\rm QCD}=\sigma^0+\Delta\sigma^{\rm QCD}=\sigma^0+\Delta\sigma^{(3)}+\Delta\sigma^{(4)}. \quad (2.32)$$

In adopting Eqs. (2.30), (2.31), and (2.32) for the numerical calculation, we use the CTEQ6M [23] PDFs.

III. NUMERICAL RESULTS AND DISCUSSION

In this section we describe and discuss the numerical results for the LO and NLO QCD corrected physical observables for the processes $pp(p\bar{p})\to t\bar{t}\gamma+X$. We take one-loop and two-loop running α_s in the LO and NLO calculations, respectively [6]. The number of active flavors is $N_f=5$, and the QCD parameters are $\Lambda_5^{\rm LO}=165$ MeV and $\Lambda_5^{\overline{\rm MS}}=226$ MeV for the LO and NLO calculations, respectively. We set the factorization scale and the renormalization scale being equal (i.e., $\mu=\mu_f=\mu_r$) and take $\mu=\mu_0=m_t$ by default unless otherwise stated. Throughout this paper, we take $m_t=171.2$ GeV and $\alpha(m_Z)^{-1}=127.918$ [6], and set quark masses $m_u=m_d=m_s=0$ and $m_c=1.3$ GeV which are the same as the input parameters used in CTEQ PDFs [23]. The colliding energies in the proton-(anti)proton center-of-mass system are

taken as $\sqrt{s} = 14$ TeV for the LHC and $\sqrt{s} = 1.96$ TeV for the Tevatron Run II.

To distinguish the photon from the jets requires the angle between the outgoing photon and jet constrained in the range of $\theta_{\gamma,\text{jet}} > \theta^{\text{cut}}_{\gamma,\text{jet}}$ (in the center-of-mass system of proton-(anti)proton). In our calculation we assume the produced (anti-)top quarks are always tagged and not effected by the phase-space cut. During our numerical calculation, we applied a number of checks to our calculations.

(1) We have compared the numerical results of the LO cross section for the process $pp \to d\bar{d} \to t\bar{t}\gamma + X$ with $\sqrt{s} = 14$ TeV by using FEYNARTS3.4/FORMCALC5.4 [20,21] packages and COMPHEP-4.4P3 program [28], and applying the Feynman and unitary gauges, separately. In the partonic luminosity integrations we adopt the CTEQ6L1 PDFs. The results are 125.1(1) fb (CompHEP, Feynman gauge), 125.0(1) fb (CompHEP, unitary gauge), 125.1(1) fb (FeynArts, Feynman gauge) and 125.1(1) fb (FeynArts, unitary gauge). It demonstrates all these results are in good agreement.

(2) We checked the UV cancellation both analytically and numerically. The IR finiteness is verified numerically after combining all the contributions from the virtual corrections, renormalization constants, real gluon/light-(anti)quark emission partonic processes and the collinear counterterms of PDFs at the NLO.

(3) We used both the LOOPTOOLS2.2 package [21] and our in-house library to check the correctness of the deductions of the tensor integrals and IR-finite numerical calculation of the scalar integral functions at a few phase-space points. Both packages are developed based on the same expressions given in Refs. [29–31], but in different codes. The numerical results are coincident within the calculation errors.

(4) The independence of the NLO correction on the soft cutoff δ_s and collinear cutoff δ_c, were proofed. Figures 7(a) and 7(b) demonstrate that the total NLO QCD correction to the $pp(p\bar{p}) \to d\bar{d} \to t\bar{t}\gamma + X$ process at the LHC does not depend on the arbitrarily chosen value of the cutoff δ_s within the calculation errors, where we take the photon transverse momentum cut $p_T^{(\gamma)} > 20$ GeV, $\theta_{\gamma,\text{jet}} > 3°$ [in the proton-(anti)proton center-of-mass system] and $\delta_c = 2 \times 10^{-6}$ in adopting the TCPSS method. In Fig. 7(a), the three-body correction [$\Delta\sigma^{(3)}$, see Eq. (2.30)], four-body correction [$\Delta\sigma^{(4)}$, see Eq. (2.31)], and the total QCD correction ($\Delta\sigma^{\text{QCD}}$) for the $pp(p\bar{p}) \to d\bar{d} \to t\bar{t}\gamma + X$ process are depicted as the functions of the soft cutoff δ_s with δ_s running from 2×10^{-5} to 2×10^{-3}. The amplified curve for the total QCD correction, $\Delta\sigma^{\text{QCD}}$, is presented in Fig. 7(b) together with calculation errors. Figures 8(a) and 8(b) show the independence of the total NLO QCD correction to the $pp(p\bar{p}) \to d\bar{d} \to t\bar{t}\gamma + X$ process on the cutoff δ_c where we take $\delta_s = 2 \times 10^{-3}$, $\theta_{\gamma,\text{jet}} > 3°$ and $p_T^{(\gamma)} > 20$ GeV. In Fig. 8(b) the amplified curve for $\Delta\sigma^{\text{QCD}}$ for the $pp(p\bar{p}) \to d\bar{d} \to t\bar{t}\gamma + X$ process is depicted. The verification that the total QCD correction $\Delta\sigma^{\text{QCD}}$ for the $pp(p\bar{p}) \to d\bar{d} \to t\bar{t}\gamma + X$ process is independent of these two cutoffs not only demonstrates the cancellation of soft/collinear IR divergencies in the total NLO QCD corrections to the processes $pp(p\bar{p}) \to d\bar{d} \to t\bar{t}\gamma + X$, but also provides an indirect check for the correctness of our

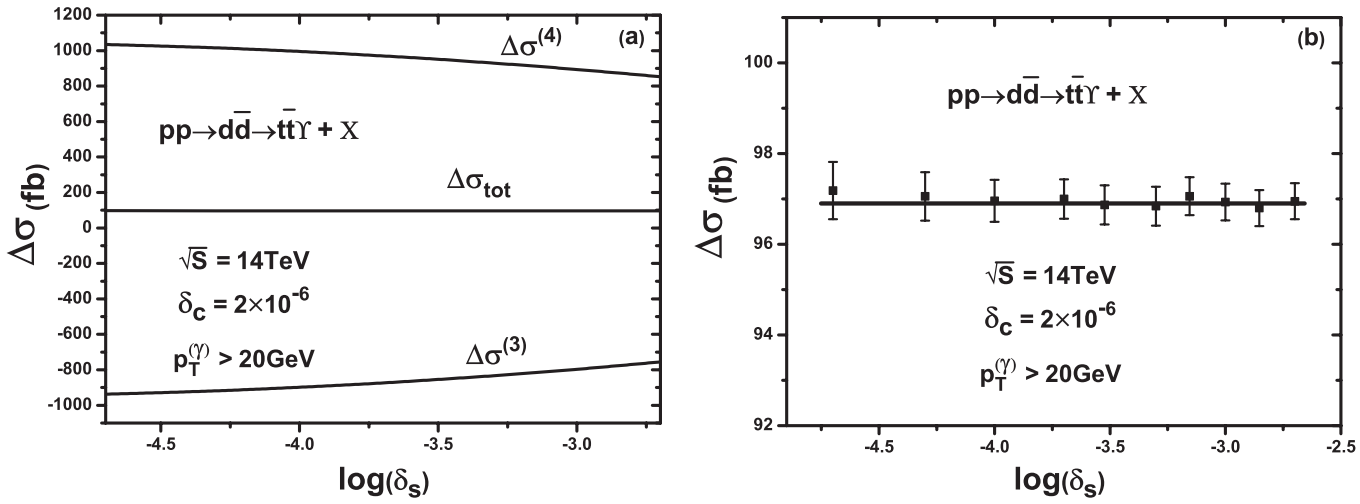

FIG. 7. (a) The dependence of the NLO QCD correction parts to the $pp(p\bar{p}) \to d\bar{d} \to t\bar{t}\gamma + X$ process on the soft cutoff δ_s at the LHC. (b) The amplified curve for the total NLO QCD correction $\Delta\sigma^{\text{QCD}}$ to the process $pp(p\bar{p}) \to d\bar{d} \to t\bar{t}\gamma + X$ in Fig. 7(a), where it includes the calculation errors.

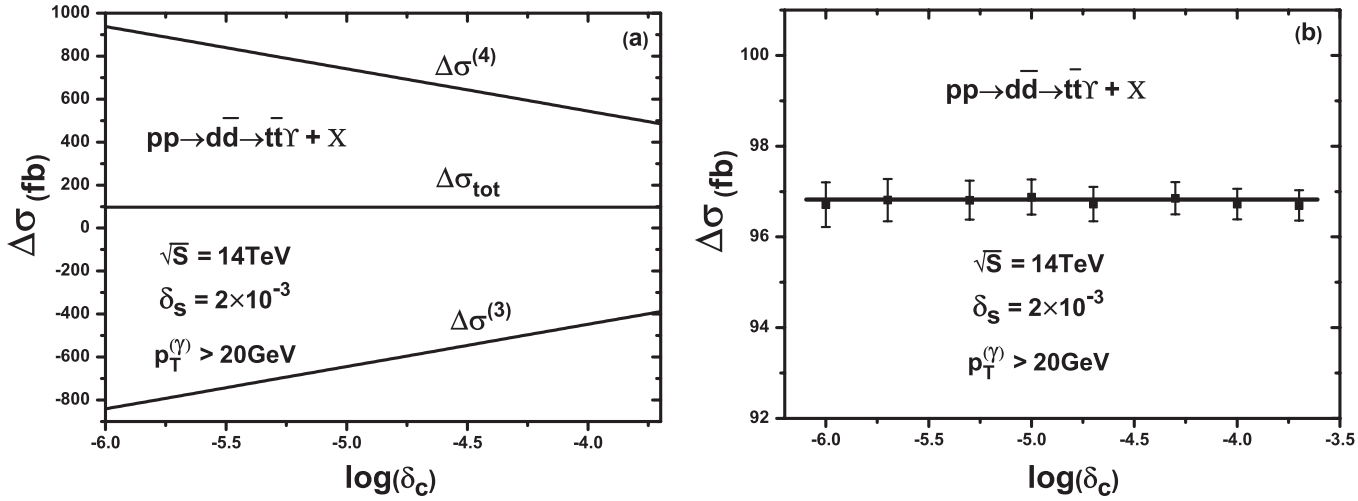

FIG. 8. (a) The dependence of the NLO QCD correction parts to the $pp(p\bar{p}) \to d\bar{d} \to t\bar{t}\gamma + X$ process on the collinear cutoff δ_c at the LHC. (b) The amplified curve for the total QCD correction $\Delta\sigma^{\rm QCD}$ to the process $pp(p\bar{p}) \to d\bar{d} \to t\bar{t}\gamma + X$ in Fig. 8(a), where it includes the calculation errors.

calculations. In further numerical calculations, we fix $p_T^{(\gamma)} > 20$ GeV, $\theta_{\gamma,\rm jet}^{\rm cut} = 3°$, $\delta_s = 10^{-3}$ and $\delta_c = \delta_s/50$, if there is no other statement.

In Figs. 9(a) and 10(a) we present the dependence of the integrated LO and the NLO QCD corrected cross sections on the renormalization/factorization scale (μ) at the LHC and Tevatron RUN II, separately. There we assume $\mu = \mu_r = \mu_f$ and define $\mu_0 \equiv m_t$. We can see that although the curves for the LO and NLO cross sections have visible variations when the energy scale μ runs from $0.1m_t$ to $3m_t$, the curves for NLO become more stable in comparison with the corresponding curves for LO. It demonstrates that the NLO QCD corrections reduce obviously the dependence of the cross section on the introduced parameter μ in the plotted μ/μ_0 value range. The corresponding total K-factor ($K \equiv \sigma^{\rm QCD}/\sigma_{\rm LO}$), the NLO QCD K-factor from the $pp(p\bar{p}) \to q\bar{q} \to t\bar{t}\gamma + X$ processes [$K_{q\bar{q}} \equiv 1 + \frac{\sum_{q=u,d,}^{s,c}(\Delta\sigma_{q\bar{q}}^{\rm QCD})}{\sigma_{\rm LO}}$], the K-factor from the $pp(p\bar{p}) \to gg \to t\bar{t}\gamma + X$ process ($K_{gg} \equiv 1 + \frac{\Delta\sigma_{gg}^{\rm QCD}}{\sigma_{\rm LO}}$) and the K-factor from the $pp(p\bar{p}) \to gq(g\bar{q}) \to t\bar{t}\gamma q(\bar{q}) + X$ processes [$K_{gq} \equiv 1 + \frac{\sum_{q=u,d,}^{s}(\Delta\sigma_{gq}^{\rm QCD} + \Delta\sigma_{g\bar{q}}^{\rm QCD})}{\sigma_{\rm LO}}$] are plotted

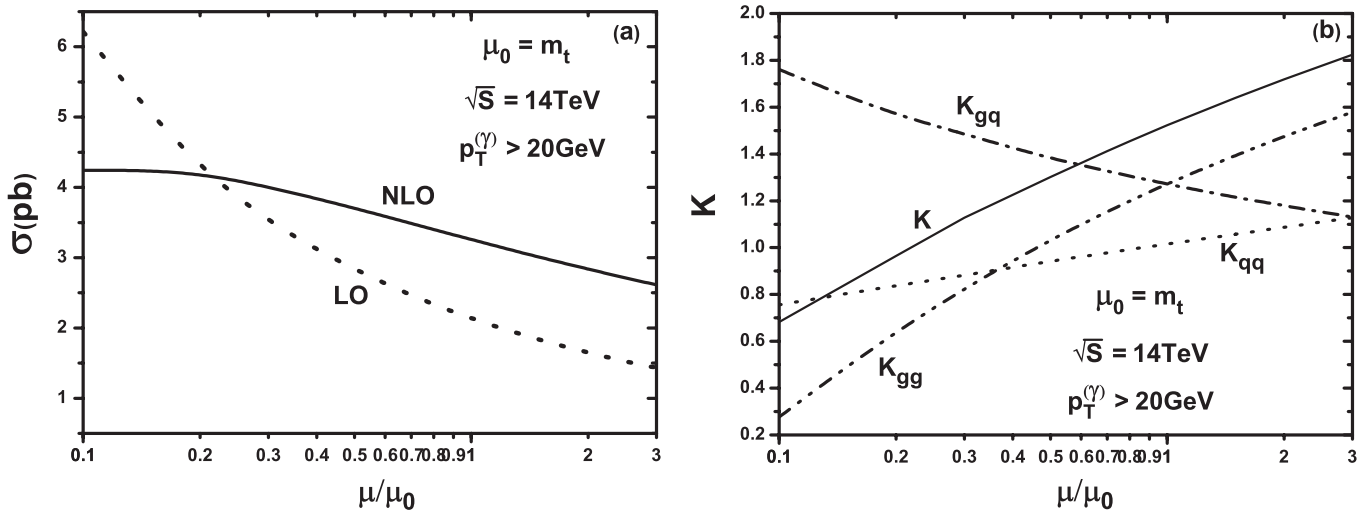

FIG. 9. (a) The dependence of the LO and NLO cross sections on the factorization/renormalization scale at the LHC. (b) The total NLO QCD K-factor for the process ($K \equiv \sigma^{\rm QCD}/\sigma_{\rm LO}$), the NLO QCD K-factor from the $p\bar{p} \to q\bar{q} \to t\bar{t}\gamma + X$ ($q = u, d, s, c$) processes [$K_{q\bar{q}} \equiv 1 + \frac{\sum_{q=u,d,}^{s,c}(\Delta\sigma_{q\bar{q}}^{\rm QCD})}{\sigma_{\rm LO}}$], the $p\bar{p} \to gg \to t\bar{t}\gamma + X$ process ($K_{gg} \equiv 1 + \Delta\sigma_{gg}^{\rm QCD}/\sigma_{\rm LO}$) and the $p\bar{p} \to gq(\bar{q}) \to t\bar{t}\gamma + X$, ($q = u, d, s$) processes [$K_{gq} \equiv 1 + \frac{\sum_{q=u,d,}^{s}(\Delta\sigma_{gq}^{\rm QCD} + \Delta\sigma_{g\bar{q}}^{\rm QCD})}{\sigma_{\rm LO}}$] versus the energy scale at the LHC.

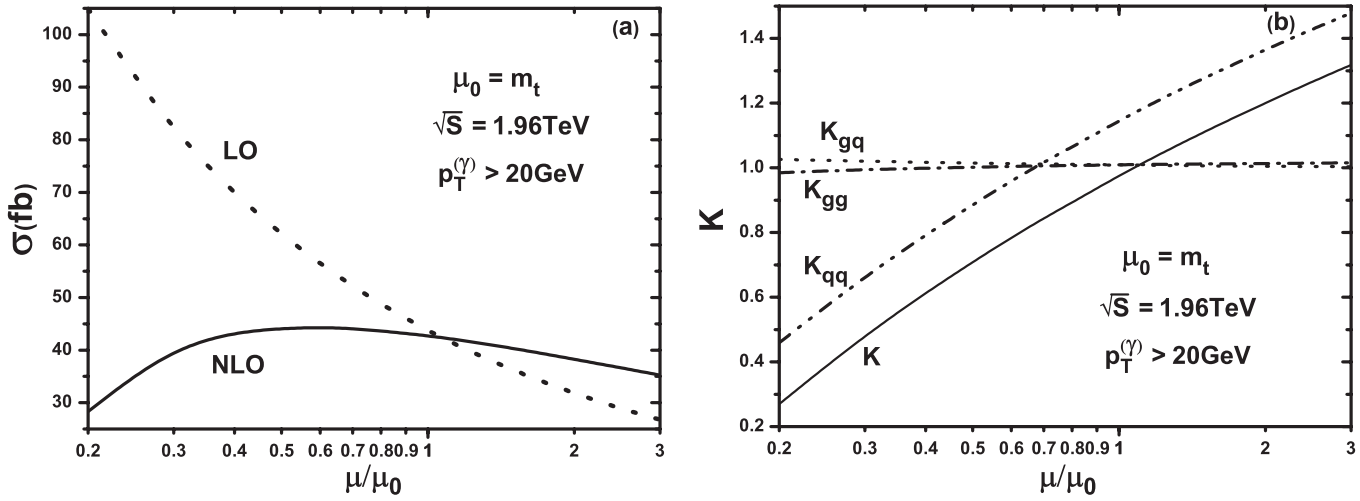

FIG. 10. (a) The dependence of the LO and NLO cross sections on the factorization/renormalization scale at the Tevatron. (b) The total NLO QCD K-factor for the process ($K \equiv \Delta\sigma^{\rm QCD}/\sigma_{\rm LO}$), the NLO QCD K-factor from the $p\bar{p} \to q\bar{q} \to t\bar{t}\gamma + X$ ($q = u, d, s, c$) processes [$K_{q\bar{q}} \equiv 1 + \frac{\sum_{q=u,d,}^{s,c}(\Delta\sigma_{q\bar{q}}^{\rm QCD})}{\sigma_{\rm LO}}$], the $p\bar{p} \to gg \to t\bar{t}\gamma + X$ process ($K_{gg} \equiv 1 + \Delta\sigma_{gg}^{\rm QCD}/\sigma_{\rm LO}$) and the $p\bar{p} \to gq(\bar{q}) \to t\bar{t}\gamma + X$, ($q = u, d, s$) processes [$K_{gq} \equiv 1 + \frac{\sum_{q=u,d,}^{s}(\Delta\sigma_{gq}^{\rm QCD} + \Delta\sigma_{g\bar{q}}^{\rm QCD})}{\sigma_{\rm LO}}$] versus the energy scale at the Tevatron.

in Fig. 9(b) for the LHC and Fig. 10(b) for the Tevatron. Figure 9(b) shows that at the LHC the integrated NLO QCD corrections always enhance the LO cross sections except in the range of $0.1 < \mu/\mu_0 < 0.21$, and the NLO QCD corrections from the $pp \to gg \to t\bar{t}\gamma + X$ and $pp \to q\bar{q} \to t\bar{t}\gamma + X$ ($q = u, d, s, c$) processes counteract the other contributions in the region of $0.1 < \mu/\mu_0 < 0.46$. Figure 9(b) shows when we take $\mu/\mu_0 = 1$, the NLO QCD correction to the $pp \to gg \to t\bar{t}\gamma + X$ process at the LHC is much larger than the correction to $pp \to q\bar{q} \to t\bar{t}\gamma + X$ processes, while Fig. 10(b) demonstrates the NLO QCD correction to the $p\bar{p} \to q\bar{q} \to t\bar{t}\gamma + X$ processes at the Tevatron is larger than that to $p\bar{p} \to gg \to t\bar{t}\gamma + X$ in the vicinity of $\mu/\mu_0 = 1$. In the further calculations, we fix $\mu = \mu_0 = m_t$.

In Table I we list the numerical results related to the data in Figs. 9(a) and 9(b) for the LHC and Figs. 10(a) and 10(b) for the Tevatron at the position of $\mu = \mu_0$. They are the results for the integrated LO and NLO QCD corrected cross sections, the total K-factor ($K \equiv \frac{\sigma^{\rm QCD}}{\sigma_{\rm LO}}$) of the process $pp(p\bar{p}) \to t\bar{t}\gamma + X$, the K-factor contributed by all the NLO QCD corrections to the $pp(p\bar{p}) \to q\bar{q} \to t\bar{t}\gamma + X$ ($q = u, d, s, c$) processes ($K_{q\bar{q}} \equiv 1 + \frac{\sum_{q=u,d,}^{s,c}(\Delta\sigma_{q\bar{q}}^{\rm QCD})}{\sigma_{\rm LO}}$), the K-factor contributed by the integrated NLO QCD correction to the $pp(p\bar{p}) \to gg \to t\bar{t}\gamma + X$ process ($K_{gg} \equiv 1 + \frac{\Delta\sigma_{gg}^{\rm QCD}}{\sigma_{\rm LO}}$) and the K-factor contributed by the corrections to the $pp(p\bar{p}) \to gq(g\bar{q}) \to t\bar{t}\gamma q(\bar{q}) + X$ processes ($K_{gq} \equiv 1 + \frac{\sum_{q=u,d,}^{s}(\Delta\sigma_{gq}^{\rm QCD} + \Delta\sigma_{g\bar{q}}^{\rm QCD})}{\sigma_{\rm LO}}$) at the LHC and Tevatron.

The LO and NLO differential cross sections of the transverse momenta for the top quark and photon at the LHC, are depicted in Fig. 11(a) and 11(b), respectively. The analogous plots at the Tevatron are depicted in Figs. 12(a) and 12(b). Figures 11(a) and 11(b) demonstrate that the NLO QCD corrections enhance significantly the differential cross sections of $p_T^{(t)}$ and $p_T^{(\gamma)}$ for the LHC, but the corrections make only a small impact on the distributions of $p_T^{(t)}$ and $p_T^{(\gamma)}$ for the Tevatron as shown in

TABLE I. The LO and NLO cross sections, the total K-factor ($K \equiv \frac{\sigma^{\rm QCD}}{\sigma_{\rm LO}}$), the K-factor contributed by the NLO QCD correction to the $pp(p\bar{p}) \to q\bar{q} \to t\bar{t}\gamma + X$ ($q = u, d, s, c$) processes ($K_{q\bar{q}} \equiv 1 + \frac{\sum_{q=u,d,}^{s,c}(\Delta\sigma_{q\bar{q}}^{\rm QCD})}{\sigma_{\rm LO}}$), the K-factor contributed by the NLO QCD correction to the $pp(p\bar{p}) \to gg \to t\bar{t}\gamma + X$ process ($K_{gg} \equiv 1 + \frac{\Delta\sigma_{gg}^{\rm QCD}}{\sigma_{\rm LO}}$), and the K-factor contributed by the corrections to the $pp(p\bar{p}) \to gq(g\bar{q}) \to t\bar{t}\gamma q(\bar{q}) + X$ ($q = u, d, s$) processes ($K_{gq} \equiv 1 + \frac{\sum_{q=u,d,}^{s}(\Delta\sigma_{gq}^{\rm QCD} + \Delta\sigma_{g\bar{q}}^{\rm QCD})}{\sigma_{\rm LO}}$) with $\mu = m_t$, $p_T^{(\gamma)} > 20$ GeV and $\theta_{\gamma,\rm jet}^{\rm cut} = 3°$ at the LHC and Tevatron.

Collider	$\sigma_{\rm LO}$	$\sigma^{\rm QCD}$	$K_{q\bar{q}}$	K_{gg}	K_{gq}	K
LHC	2.141(2) (pb)	3.256(6) (pb)	1.014	1.272	1.272	1.521
Tevatron	43.79(4) (fb)	42.80(6) (fb)	1.148	1.009	1.009	0.977

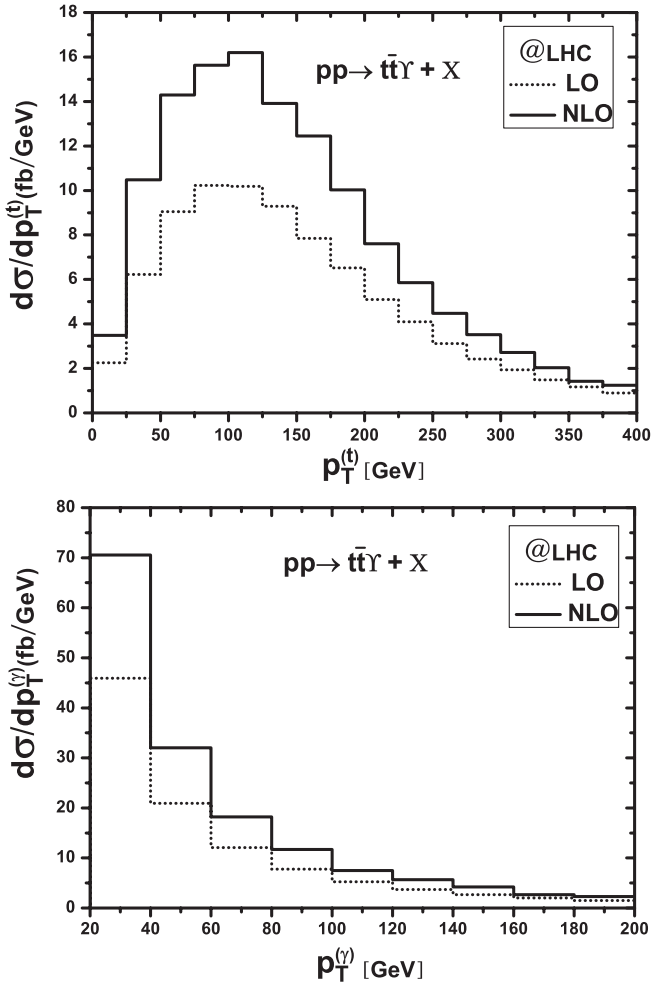

FIG. 11. The LO and NLO distributions of the transverse momenta of the top quark and photon taking $\mu = m_t$, $p_T^{(\gamma)} > 20$ GeV and $\theta_{\gamma,\mathrm{jet}}^{\mathrm{cut}} = 3°$ at the LHC. (a) for the top quark, (b) for the photon.

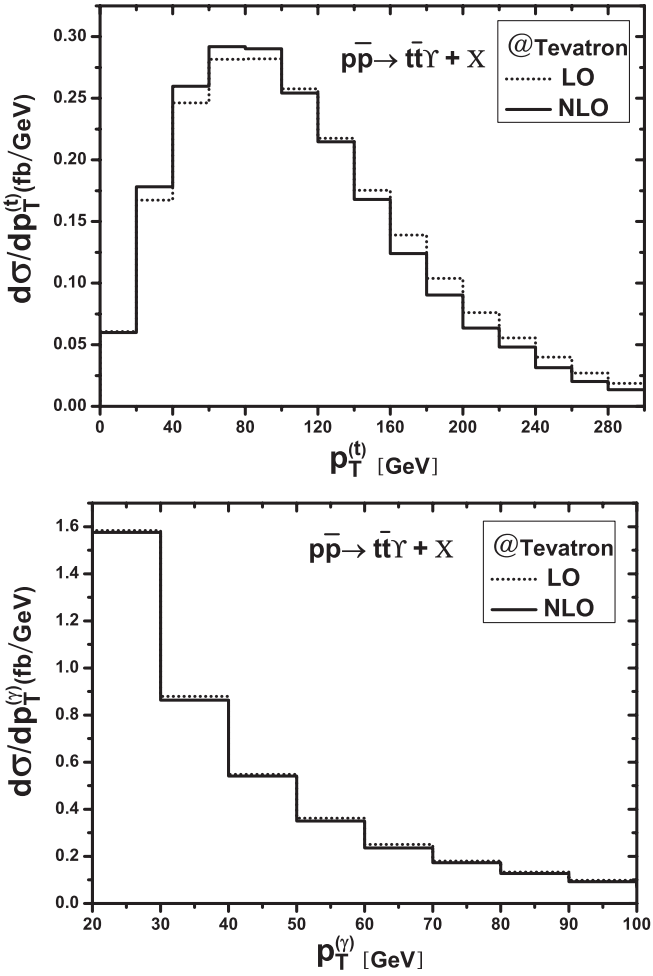

FIG. 12. The LO and NLO distributions of the transverse momenta of the top quark and photon taking $\mu = m_t$, $p_T^{(\gamma)} > 20$ GeV and $\theta_{\gamma,\mathrm{jet}}^{\mathrm{cut}} = 3°$ at the Tevatron. (a) for the top quark, (b) for the photon.

Figs. 12(a) and 12(b). In Figs. 12(a) and 12(b) the NLO corrections at the Tevatron suppress the LO distribution of $p_T^{(t)}$ a little bit except in the range of 20 GeV $< p_T^{(t)} <$ 100 GeV, while the corrections slightly reduce the LO differential cross section of $p_T^{(\gamma)}$ in the whole plotted $p_T^{(\gamma)}$ range. From the distributions of $p_T^{(\gamma)}$ in both Fig. 11(b) and 12(b), we can conclude that most of the photons in the events of $pp(p\bar{p}) \to t\bar{t}\gamma + X$ are produced in low transverse momentum range at the LHC and Tevatron.

We adopt the definitions of the LO and NLO top-quark charge asymmetries in Ref. [32], i.e.,

$$A_{\mathrm{FB,LO}}^{t} = \frac{\sigma_{\mathrm{LO}}^{-}}{\sigma_{\mathrm{LO}}^{+}},$$
$$A_{\mathrm{FB,NLO}}^{t} = \frac{\sigma_{\mathrm{LO}}^{-}}{\sigma_{\mathrm{LO}}^{+}}\left(1 + \frac{\Delta\sigma_{\mathrm{NLO}}^{-}}{\sigma_{\mathrm{LO}}^{-}} - \frac{\Delta\sigma_{\mathrm{NLO}}^{+}}{\sigma_{\mathrm{LO}}^{+}}\right), \tag{3.1}$$

In Eq. (3.1) the notations $\sigma_{\mathrm{LO}}^{\pm}$ have the explicit definitions as

$$\sigma_{\mathrm{LO}}^{\pm} = \sigma_{\mathrm{LO}}(y_t > 0) \pm \sigma_{\mathrm{LO}}(y_t < 0), \tag{3.2}$$

where cross sections $\sigma_{\mathrm{LO}}(y_t > 0)$ and $\sigma_{\mathrm{LO}}(y_t < 0)$ get the contributions from the top quarks in the forward and backward hemispheres at LO, respectively, [The forward direction is defined as the orientation of incoming proton (P_1).], $\Delta\sigma_{\mathrm{NLO}}^{\pm}$ denote the NLO QCD contributions to the cross sections $\sigma_{\mathrm{LO}}^{\pm}$. By using our program with the same conditions as used in Table 3.1 of Ref. [32], we calculated the LO cross section and the top-quark charge asymmetry for the process $p\bar{p} \to t\bar{t} + \mathrm{jet} + X$ at the Tevatron. We obtained $\sigma_{\mathrm{LO}} = 1.582(2)$ pb and $A_{\mathrm{FB,LO}}^{t} = -7.70(6)\%$ by taking $p_{T,\mathrm{jet,cut}} = 20$ GeV and $\mu = m_t$, which are coincident with those in Table 3.1 of Ref. [32].

In Table II we present the results of LO and NLO cross sections (σ_{LO} and σ^{QCD}) and LO and NLO forward-backward charge asymmetries of the top quark ($A_{\mathrm{FB,LO}}^{t}$ and $A_{\mathrm{FB,NLO}}^{t}$) for the process $p\bar{p} \to t\bar{t}\gamma + X$ at the

TABLE II. The LO and NLO cross sections and the LO and NLO forward-backward charge asymmetries of the top quark at the Tevatron with $\mu = m_t$, $\theta^{\rm cut}_{\gamma,\rm jet} = 3°$ (in the proton-antiproton center-of-mass system) and $p^{(\gamma)}_{T,\rm cut} = 20$ GeV, 30 GeV, 40 GeV, respectively.

$p^{(\gamma)}_{T,\rm cut}$ (GeV)	$\sigma_{\rm LO}$ (fb)	$\sigma^{\rm QCD}$ (fb)	$A^t_{\rm FB,LO}$ (%)	$A^t_{\rm FB,NLO}$ (%)
20	43.79(4)	42.80(6)	−17.24(7)	−11.41(8)
30	27.88(2)	26.94(4)	−18.21(8)	−11.52(9)
40	19.09(1)	18.26(2)	−18.85(8)	−11.90(9)

Tevatron. There we set $\mu = m_t$, $\theta^{\rm cut}_{\gamma,\rm jet} = 3°$, and the photon transverse momentum cut $p^{(\gamma)}_{T,\rm cut} = 20$ GeV, 30 GeV and 40 GeV, respectively. The numerical results in the table show the NLO QCD correction reduces evidently the absolute values of LO asymmetry, e.g., in the case of $p^{(\gamma)}_{T,\rm cut} = 20$ GeV, the LO asymmetry $|A^t_{\rm FB,LO}| = 17.24\%$ is cut down to $|A^t_{\rm FB,NLO}| = 11.41\%$ by the NLO QCD corrections. The absolute values for both LO and NLO asymmetries are quantitatively increased a little bit with the growing of $p^{(\gamma)}_{T,\rm cut}$ from 20 GeV to 40 GeV.

IV. SUMMARY

In this paper we calculate the complete NLO QCD corrections to the top-pair production associated with a photon at the LHC and Tevatron Run II. We investigate the dependence of the LO and NLO QCD corrected integrated cross sections on the factorization/renormalization energy scale. We present also the predictions for LO and NLO QCD corrected charge asymmetries of top quarks at the Tevatron, and the LO and NLO differential cross sections at the LHC and Tevatron. We find from our numerical results that the NLO QCD radiative corrections obviously modify the LO charge asymmetry of top-quark, integrated, and differential cross sections. And the uncertainty of the LO cross section due to the introduced unphysical energy scale μ, is significantly improved by including NLO QCD corrections. Our numerical results show that by taking $\mu = m_t$ the K-factors of the NLO QCD corrections at the LHC and Tevatron RUN II are 1.524 and 0.977, respectively.

ACKNOWLEDGMENTS

This work was supported in part by the National Natural Science Foundation of China (No. 10875112, No. 10675110).

[1] F. Abe *et al.* (CDF Collaboration), Phys. Rev. Lett. **74**, 2626 (1995).
[2] S. Abachi *et al.* (D0 Collaboration), Phys. Rev. Lett. **74**, 2632 (1995).
[3] S. L. Glashow, Nucl. Phys. **22**, 579 (1961); S. Weinberg, Phys. Rev. Lett. **19**, 1264 (1967); A. Salam, *Proc. 8th Nobel Symposium Stockholm 1968*, edited by N. Svartholm (Almquist and Wiksells, Stockholm, 1968), p. 367; H. D. Politzer, Phys. Rep. **14**, 129 (1974).
[4] P. W. Higgs, Phys. Rev. Lett **12**, 132 (1964); Phys. Rev. Lett. **13**, 508 (1964); Phys. Rev. **145**, 1156 (1966); F. Englert and R. Brout, Phys. Rev. Lett. **13**, 321 (1964); G. S. Guralnik, C. R. Hagen, and T. W. B. Kibble, Phys. Rev. Lett. **13**, 585 (1964); T. W. B. Kibble, Phys. Rev. **155**, 1554 (1967).
[5] Tevatron Electroweak Working Group (CDF and D0 Collaborations), Report Nos. Fermilab-TM-2347-E, TEVEWWG/top 2006/01, CDF-8162, D0-5064.
[6] C. Amsler *et al.*, Phys. Lett. B **667**, 1 (2008).
[7] D. Chakraborty, J. Konigsberg, and D. Rainwater, Annu. Rev. Nucl. Part. Sci. **53**, 301 (2003).
[8] M. C. Smith and S. S. Willenbrock, Phys. Rev. Lett. **79**, 3825 (1997).
[9] T. Abe *et al.* (American Linear Collider Working Group), in *Proc. of the APS/DPF/DPB Summer Study on the Future of Particle Physics(Snowmass 2001)*, edited by N. Graf.
[10] U. Baur, A. Juste, L. H. Orr, and D. Rainwater, Phys. Rev. D **71**, 054013 (2005).
[11] K. Hagiwara, H. Murayama, and I. Watanabe, Nucl. Phys. **B367**, 257 (1991); Dai Lei, Ma Wen-Gan, Zhang Ren-You, Guo Lei, and Wang Shao-Ming, Phys. Rev. D **78**, 094010 (2008).
[12] Dong Chuan-Fei, Ma Wen-Gan, Zhang Ren-You, Guo Lei, and Wang Shao-Ming, arXiv:0812.4728v1.
[13] W. Bernreuther, J. Phys. G **35**, 083001 (2008).
[14] W. Bernreuther, T. Schöder, and T. N. Pham, Phys. Lett. B **279**, 389 (1992).
[15] R. S. Chivukula, S. B. Selipsky, and E. H. Simmons, Phys. Rev. Lett. **69**, 575 (1992); R. S. Chivukula, E. H. Simmons, and J. Terning, Phys. Lett. B **331**, 383 (1994); K. Hagiwara and N. Kitazawa, Phys. Rev. D **52**, 5374 (1995); U. Mahanta, Phys. Rev. D **55**, 5848 (1997); **56**, 402 (1997).
[16] C. T. Hill and E. H. Simmons, Phys. Rep. **381**, 235 (2003).**390**, 553(E) (2004).
[17] C. F. Berger, M. Perelstein, and F. Petriello, Report Nos. MADPH-05-1251, SLAC-PUB-11589; T. Abe *et al.* (American Linear Collider Working Group), in *Proc. of the APS/DPF/DPB Summer Study on the Future of Particle Physics(Snowmass 2001)*, edited by N. Graf.
[18] U. Baur, A. Juste, L. H. Orr, and D. Rainwater, Phys. Rev. D **71**, 054013 (2005).
[19] A. Lazopoulos, T. McElmurry, K. Melnikov, and F. Petriello, Phys. Lett. B **666**, 62 (2008); A. Lazopoulos, K. Melnikov, and F. Petriello, Phys. Rev. D **77**, 034021

(2008).
[20] T. Hahn, Comput. Phys. Commun. **140**, 418 (2001).
[21] T. Hahn and M. Perez-Victoria, Comput. Phys. Commun. **118**, 153 (1999).
[22] S. Dittmaier, Nucl. Phys. **B675**, 447 (2003); W. Beenakk and S. Dittmaier *et al.*, Nucl. Phys. **B653**, 151 (2003).
[23] J. Pumplin *et al.*., J. High Energy Phys. 07 (2002) 012; D. Stump *et al.*, J. High Energy Phys. 10 (2003) 046.
[24] B. W. Harris and J. F. Owens, Phys. Rev. D **65**, 094032 (2002).
[25] W. Beenakker, H. Kuijf, W. L. van Neerven, and J. Smith, Phys. Rev. D **40**, 54 (1989); W. Beenakker, S. Dittmaier, M. Kramer, B. Plumper, M. Spira, and P. M. Zerwas, Phys. Rev. Lett. **87**, 201805 (2001); Nucl. Phys. **653**, 151 (2003).
[26] G. Altarelli and G. Parisi, Nucl. Phys. **126**, 298 (1977).
[27] T. Kinoshita, J. Math. Phys. (N.Y.) **3**, 650 (1962); T. D. Lee and M. Nauenberg, Phys. Rev. **133**, B1549 (1964).
[28] E. Boos and V. Bunichev *et al.* (CompHEP Collaboration), Nucl. Instrum. Methods Phys. Res., Sect. A **534**, 250 (2004).
[29] G.'t Hooft and M. Veltman, Nucl. Phys. **153**, 365 (1979).
[30] A. Denner, U Nierste, and R Scharf, Nucl. Phys. **367**, 637 (1991).
[31] A. Denner and S. Dittmaier, Nucl. Phys. **658**, 175 (2003).
[32] S. Dittmaier, P. Uwer, and S. Weinzierl, Eur. Phys. J. C **59**, 625 (2009).